FLOOD MAPPING WITH SAR AND MULTI-SPECTRAL REMOTE SENSING IMAGES BASED ON WEIGHTED EVIDENTIAL FUSION

Xi Chen[1] Yaokui Cui[1] Changjun Wen[2] Mingxuan Zheng[2] Yuan Gao[2] Jing Li[3]*

[1] School of Earth and Space Sciences, Peking University, Beijing 100871, China;
[2] Information Center of Ministry of Civil Affairs of the People's Republic of China, Beijing 100721, China;
[3] Faculty of Geographical Science, Beijing Normal University, Beijing 100875, China

IGARSS 2020 - 2020 IEEE International Geoscience and Remote Sensing Symposium | 978-1-7281-6374-1/20/$31.00 ©2020 IEEE | DOI: 10.1109/IGARSS39084.2020.9324158

ABSTRACT

Synthetic Aperture Radar (SAR) and Multi-spectral (MS) remote sensing images are commonly used for flood mapping. SAR images can provide valid backscattering measurements of inundated areas through cloud cover, while MS data is able to monitor the spectral changes of ground surface, but usually affected by clouds. The complementary characteristics of the two data indicate the potential of their combining application for flood monitoring in emergency. This paper proposes a novel weighted evidential fusion method to take full advantages of the SAR and MS data for change detection during the flood. First, pre-processing and classification are performed with the SAR and MS data, independently. Second, a modified PCR6 rule for evidential fusion is proposed, which introduces the confusion matrixes to calculate the weight of evidences so that the conflicting degree in the fusion process can be reduced. Then, the flood inundating, standing and receding patterns are identified, which can be used to describe the flooding process in details. Practically, the proposed method is applied to flood mapping of the *Typhoon Rumbia* in 2018, in Shouguang City, China. The experiments show that the proposed fusion scheme efficiently use both of the SAR and MS data, and improve the flood mapping accuracy.

Index Terms— SAR, multi-spectral, change detection, evidential fusion, flood monitoring, remote sensing

1. INTRODUCTION

Rapid and accurate mapping of floods is important for flood prevention, emergency management, and post-disaster reconstruction [1]. The incremental big earth observation (EO) data and remote sensing techniques have demonstrated great potential in near-real time and synergistic flood mapping. Synthetic Aperture Radar (SAR) is particularly useful for flood mapping especially in rainy or cloudy weather, because of its capability to monitor land surface changes in almost any weather conditions [2]. However, land surface water is not always easy to be detected in SAR images when the water is stirred by storms (which lead to high surface roughness), covered by tall plants, or in topography shadows [3]. Multi-spectral (MS) remote sensing images are complementary with the SAR data. MS images can be used to detect spectral changes of land surface resulting from water coverage. However, clouds or shadows are usually considered as defective information, and limits their application on flood mapping using multi-temporal MS data [4]. Hence, the combining use of SAR and MS satellite imagery can be prospective and effective for inundation detection and flood mapping. Many methods have been proposed for mapping flood inundation only use SAR or MS images [2]. However, the combining use of SAR and MS images for flood mapping, especially for detecting the flood inundating, standing, and receding patterns with multi-temporal data is still challenging. The main difficulty lies on the uncertainty and conflicting information that exist between the SAR and MS data.

The evidential fusion method, generally known as a fusion scheme on the decision level, can flexibly combine multiple imprecise or uncertain evidences and has been successfully applied to change detection with multi-source remote sensing data in emergency situations [5]. Even though the method is usually more effective than the traditional Bayesian ones, the existing evidential fusion algorithms neglect the difference of overall accuracy of the evidences, and lead to low accuracy when fusing multi-source data with high conflict degree [6]. This research develops an innovative weighting scheme based on PCR6 rule of the evidential fusion method using multi-temporal SAR and MS images, and applies the method to detect the inundating, standing, and receding patterns in the whole flooding process.

2. STUDY AREA AND DATASETS

2.1. Study area

Shouguang city is a famous source area of vegetable in eastern China. Many villages in low-lying parts of the city was hit by floods caused by the Typhoon Rumbia in 2018. In particular, from August 17 to 20, 2018, Rumbia brought extreme rainfall after its landing and posed great threat to the upper reservoirs, and the reservoirs increased flood discharge after August 20 to prevent from greater loss. The flood submerged many villages, farms and rendered hundreds of people in need of shelter (Fig. 1).

2.2. Datasets and Pre-processing

To retrospect the flooding process, multi-temporal SAR and MS images are obtained and pre-processed using the Google Earth Engine (GEE). The pre-disaster, during flood, and post-disaster data used in this study include SAR images

Authorized licensed use limited to: University of Cape Town. Downloaded on May 17,2021 at 19:01:25 UTC from IEEE Xplore. Restrictions apply.

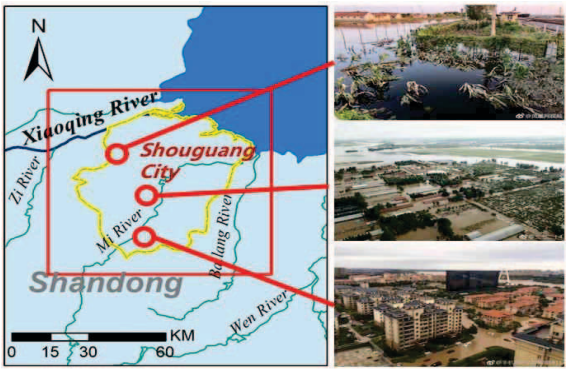

Fig. 1 Location of the study area and local pictures

from Sentinel-1 A/B satellite with VV and VH polarization, MS images from Sentinel-2 satellite with 12 bands, and Landsat8-OLI images with 9 bands (Listed in Table 1). Pre-processing include radiation correction, cloud detection and image resampling. After pre-processing, nine images of 8000×8000 pixels (in 10 meters' resolution) are derived.

3. METHODOLOGY

3.1. Classification and accuracy evaluation

SAR and MS images are suitable for identifying different land cover, which are both redundant and complementary. In this paper, the Random Forest (RF) algorithm is used for classification, and manually interpreted samples are obtained for training the classifier and evaluating the result accuracy. Each image is classified into four categories: Open Water (θ_1), Wet Land (θ_2), Dry Land (θ_3), and Unknown (θ_4). After classification, cross validation is performed to evaluate the accuracy using the testing samples. Then, the confusion matrix of every classification is derived, which will be used as input parameter in the following evidential fusion process. The overall confusion matrix of SAR and MS classification is presented in Table 2.

3.2. Weighted evidential fusion for change detection

According to the confusion matrixes of classification, the SAR images performs better than MS data in classifying Open Water and Dry Land. While MS images can be used to classify Wet Land, which has significant spectral difference with other land cover types, but MS images are easy to be affected by clouds and shadows. The original Dempster-Shafer Evidential Fusion method, known as a decision level fusion scheme, only considers the belief degree of each class in the input evidences, but neglects the overall reliability of each evidence. This will lead to high conflicting degree when fusing evidences that derived from data sources with great difference of overall accuracy, such as SAR and MS images. Therefore, a weighted evidential fusion scheme is developed in this research. The proposed scheme uses the confusion matrixes of classification results to modify the parameters of the evidential fusion rule. The global workflow of the proposed method is shown in Fig. 3 and is detailed as follows.

3.2.1 Definitions of change vectors

The transfer between the classified land cover categories can be used to describe the flooding process, and three land cover change patterns is identified using change vectors,

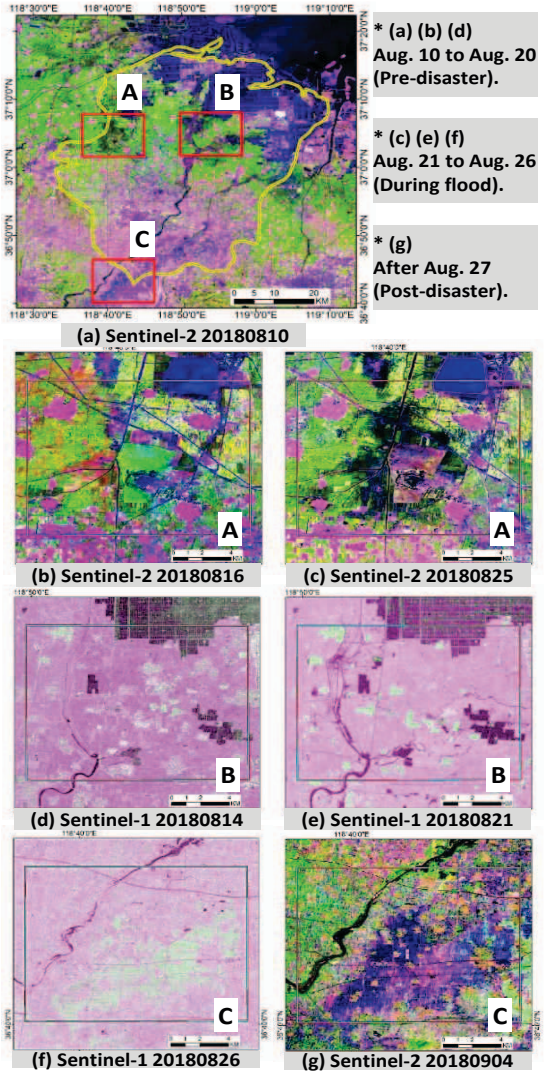

Fig. 2 Part of the remote sensing data used in this study. The images correspond to the list in Table. 1, the data sources and the locations are marked in sub-figure (a).

Table 1. List of remote sensing images used in this study.

Date of image acquisition (During Aug. and Sep., 2018)		Data source		
		Sentinel-1	Sentinel-2	Landsat8
Pre-disaster	Aug. 10		●	
	Aug. 14	●		
	Aug. 16		●	
During flood	Aug. 21	●		
	Aug. 25		●	
	Aug. 26	●		
Post-disaster	Sep. 01	●		●
	Sep. 04		●	

* Symbol ● represents image obtained in this study.

Table 2. The overall confusion matrixes of classification results.

Classified land cover with RF	SAR (Unit: %) (Ground truth land cover)				MS (Unit: %) (Ground truth land cover)			
	θ_1	θ_2	θ_3	θ_4	θ_1	θ_2	θ_3	θ_4
Open Water (θ_1)	**95.76**	0	0	—	**76.58**	22.01	4.36	0.05
Wet Land (θ_2)	0	45.23	10.98	—	11.46	**74.93**	4.36	0.41
Dry Land (θ_3)	4.24	**54.77**	**89.02**	—	6.45	2.04	**89.78**	5.05
Unknown (θ_4)	—	—	—	—	5.51	1.02	1.51	**94.49**

* The overall confusion matrixes measure the classified and ground truth land cover type using all of the classification results.

Authorized licensed use limited to: University of Cape Town. Downloaded on May 17,2021 at 19:01:25 UTC from IEEE Xplore. Restrictions apply.

namely Flood inundating pattern (P_1), Flood standing pattern (P_2), and Flood receding pattern (P_3). Denoting change vector $<\theta_x,\theta_y>$ means the pre- and post- change land cover categories are θ_x and θ_y respectively, where θ_x and θ_y ($x,y=1,2,3$) represent any of the three land cover types, namely Open Water (θ_1), Wet Land (θ_2), Dry Land (θ_3). The change patterns are symbolic represented as follows.

(1) Flood inundating: $P_1 =<\theta_3,\theta_2>\bigcup<\theta_3,\theta_1>\bigcup<\theta_2,\theta_1>$;

(2) Flood standing: $P_2 =<\theta_1,\theta_1>\bigcup<\theta_2,\theta_2>\bigcup<\theta_3,\theta_3>$;

(3) Flood receding: $P_3 =<\theta_1,\theta_2>\bigcup<\theta_1,\theta_3>\bigcup<\theta_2,\theta_3>$;

Where the flood standing pattern can be more detailed described as Unchanged Open Water $<\theta_1,\theta_1>$, Unchanged Wet Land $<\theta_2,\theta_2>$, and Not Flooded Land $<\theta_3,\theta_3>$.

3.2.2 Belief degree measurement of the flood patterns

According to the Dempster-Shafer Theory (DST) for evidential fusion, a Basic Belief Assignment (BBA) function can be used to measure the belief degree of evidences, which are consist of the detected change vectors $<\theta_x,\theta_y>$ in this study. The user's accuracy (UA) of each classification is used to calculate the BBA values as in [3]:

$$UA_t(x,i)=p_{xi}\Big/\sum_i p_{xi} \tag{1}$$

Where $x,y,i,j\in\{1,2,3\}$, p_{xi} is the element of row x and column i in the confusion matrix, which means the number of pixels that predicated as class x while its ground truth is class i. There is $t\in\{t_0,t_1\}$, t_0 and t_1 indicate the time of pre-change and post-change that the data acquired, respectively. Then, the BBA values of the flood patterns are calculated as follows:

$$\begin{cases} m(P_1)=\sum_{i>j} UA_{t0}(x,i)\cdot UA_{t1}(y,j) \\ m(P_2)=\sum_{i=j} UA_{t0}(x,i)\cdot UA_{t1}(y,j) \\ m(P_3)=\sum_{i=j} UA_{t0}(x,i)\cdot UA_{t1}(y,j) \end{cases} \tag{2}$$

Where $m(P_1)$, $m(P_2)$ and $m(P_3)$ measure the belief degree of Flood inundating (P_1), Flood standing (P_2), and Flood receding (P_3) patterns. With a pair of pre-change (t_0) and post-change(t_1) images, a change vector can be constructed as an evidence for every pixel in the flood map. Then, the BBA values of the change vector measures the belief degree of the evidence, which can be written as an array.

$$E=[m(P_1),m(P_2),m(P_3)] \tag{3}$$

3.2.3 Evidential fusion based on modified PCR6 rule

Considering more pairs of t_0 and t_1 remote sensing data, the data come from classification results of SAR or MS images. And then, many BBA arrays of evidences should be fused for each pixel, until the final flood map is derive. For example, there are three pre-disaster images and one image of Aug. 21 (Table 1), there will be three BBA arrays of evidences to be fused for each pixel. The main difficulty in fusing evidences from both SAR and MS images is the inevitable systematic classification error that will lead to conflict in the fusing process.

The fusion methods of multiple BBA arrays of evidences are called evidential fusion rules, and many rules have been provided since the DST was proposed. The 6th rule of Proportional Conflict Redistributions rules (PCR6) is newly developed, and is more suitable than Dempster's rule in combining high conflicting information [6]. However, the PCR6 rule still need modification when fusing evidences from both SAR and MS images, because the difference of classification accuracy with both SAR and MS images is much greater than that only uses classification results from either SAR or MS data. Hence, in this study the overall reliability of every input evidence should not be equal, the Overall Accuracy (OA) of different classification is, therefore, introduced as weights in PCR6 rule for different evidences.

The overall accuracy (OA) of a classification is as follows:

$$\mathrm{OA}_t=\sum_i p_{ii}\Big/\sum_{i,j} p_{ij} \tag{4}$$

Where $t\in\{t_0,t_1\}$, and p_{ij} is the element of confusion matrix in row i and column j.

Considering the fusing process of two evidences $E1$ and $E2$ that are represented as Eq.(3). For each evidence, there is a pair of overall accuracy values measuring the pre- and post-change classification accuracy, denoted as OA_{t0} and OA_{t1}, respectively. The weights of the two evidences are as follows:

$$w_1=OA_{t0}^{E1}\cdot OA_{t1}^{E1},\ w_2=OA_{t0}^{E2}\cdot OA_{t1}^{E2} \tag{5}$$

Then, the BBA values of the two evidences can be modified as follows:

$$M_1(A_i)=\frac{w_1 m_{E1}(P_i)}{w_1+w_2},\ M_2(A_i)=\frac{w_2 m_{E2}(P_i)}{w_1+w_2} \tag{6}$$

Where $m_{E1}(P_i)$ and $m_{E2}(P_i)$ represent the BBA values of change pattern P_i in evidences $E1$ and $E2$, respectively. For the original PCR6 rule, there is $w_1=w_2=1$. Then, the basic modified PCR6 rule for fusing two evidences is as follows:

$$M_{PCR6}(C)=M_1\oplus M_2=\sum_{A_i\cap B_j=C} M_1(A_i)M_2(B_j)+\sum_{X_i\cap C=\varnothing}\mathrm{K}(X_i,C) \tag{7}$$

$$\mathrm{K}(X_i,C)=\frac{M_1(C)^2\cdot M_2(X_i)}{M_1(C)+M_2(X_i)}+\frac{M_2(C)^2\cdot M_1(X_i)}{M_1(X_i)+M_2(C)} \quad (M_1(C)+M_2(X_i)\neq 0,\ M_1(X_i)+M_2(C)\neq 0) \tag{8}$$

Where $\mathrm{K}(X_i,C)\in[0,1]$ measures the conflict and uncertain degree when fusing evidences $E1$ and $E2$. And $C=A_i\bigcap B_j$, $A_i, B_j, X_i\subseteq\{P_1,P_2,P_3\}$, which represents the conjunctive consensus of possible change patterns. More evidences for each pixel can be fused one by one iteratively using Eq.(7) and (8), as $M_{PCR6}(C)$ that fused by the previous evidences can be considered as a new BBA value like M_1 and M_2.

3.2.4 Determine the flood patterns of pixels on the map

After evidential fusion, an array of fused BBA values can be derived for each pixel in a flooding map, representing the belief degree on different flood patterns based on existing evidences. Then, the widely used "maximum of belief" rule is applied to every pixel on the map, and this rule chooses the flood pattern with the maximum fused BBA value as the determined pattern on the map [3]. Finally, the flooding map can be derived. The global workflow is summarized in Fig.3.

4. RESULTS AND CONCLUSIONS

4.1. Results

The flood process in the study was divided into three phases, namely pre-disaster (Aug. 10 to Aug. 20), during flood (Aug. 21 to Aug. 26), and post-disaster (Aug. 27 to Sep. 4). Five flood patterns were identified as the frame of discernment in the evidential fusion framework, including

Authorized licensed use limited to: University of Cape Town. Downloaded on May 17,2021 at 19:01:25 UTC from IEEE Xplore. Restrictions apply.

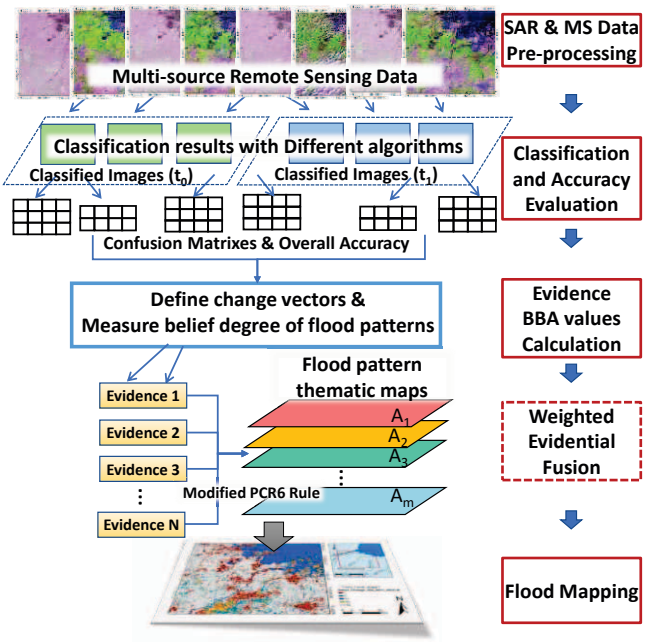

Fig. 3 Global workflow of the proposed method.

Flood Inundation, Flood Receding, Unchanged Open Water, Unchanged Wet Land, and Not Flooded Land. The flood maps of the study area during Aug. 10 and Sep. 4 is shown in Fig. 4. The flood maps illustrate the ratio of flood patterns in the three phases (Inundating: Unchanged: Receding): 9:78:13 (Pre-disaster), 13:79:8(During flood), 1:84:15(Post-disaster).

Four methods were introduced for comparison, including (I) the original Dempster-Shafer (D-S) rule, (II) the Dubois-Prade rule, (III) the original PCR6 rule, and (IV) the proposed modified PCR6 rule, and the "maximum of belief" rule was applied as the determination rule for the sake of fairness [5][6]. The results were verified based on manual interpretation and reports provided by local volunteers. Then, the mean values of user's accuracy, overall accuracy, and Kappa coefficient in the three maps are listed in Table 3. The results show that the proposed method achieves the best overall accuracy (higher than 84%, see Table 3) among all of the compared methods, and indicates the effectiveness of modifying the weights of evidences when fusing SAR and MS remote sensing data.

4.2 Conclusions

Three main conclusions can be made in this paper.

(1) The proposed weighted evidential fusion method provides an efficient way to fuse the SAR and MS data for flood mapping, and performs better than the original D-S rule, the Dubois-Prade rule, and the original PCR6 rule.

(2) The frame of discernment identified in this study, including the flood inundating, standing and receding patterns show significant spatial distribution change during the pre-disaster, during flood, and post-disaster phases.

(3) The details in the flooding map provided in this study with the proposed method can be useful for flood prevention, risk zonation, emergency management, and reconstruction.

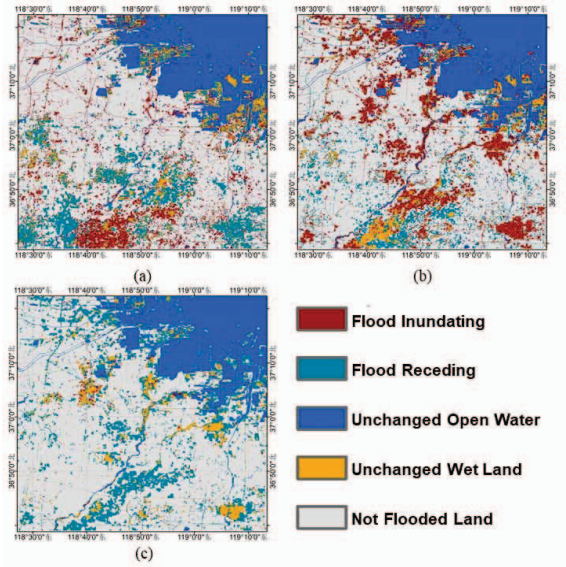

Fig. 4 Flood map of the study area. Flood process of (a) Aug. 10 to Aug. 20, (b) Aug. 21 to Aug. 26, and (c) Aug. 27 to Sep. 4.

Table 3. Flood mapping accuracy evaluation with different data sources and different algorithms.

	Flood process	Method (*I*)	(*II*)	(*III*)	(*IV*)
User's accuracy (%)	Flood Inundating	52.21	71.65	70.76	**75.39**
	Flood Receding	61.86	62.41	75.76	**77.43**
	Unchanged Open Water	85.46	57.53	**89.69**	**89.26**
	Unchanged Wet Land	79.31	82.19	78.93	**83.95**
	Not Flooded Land	69.90	76.06	76.64	**82.06**
Overall accuracy (%)		65.35	73.50	74.86	**84.56**
Kappa coefficient		0.4513	0.6362	0.5221	**0.6716**

4. REFERENCES

[1] Cian F, Marconcini M, Ceccato P. "Normalized Difference Flood Index for rapid flood mapping: Taking advantage of EO big data". *Remote Sensing of Environment*. 209, pp. 712-730, 2018.

[2] Tong X, Luo X, Liu S, et al. "An approach for flood monitoring by the combined use of Landsat 8 optical imagery and COSMO-SkyMed radar imagery". *ISPRS Journal of Photogrammetry & Remote Sensing*. 136, pp. 144-153, 2018.

[3] Chen X, Li J, Zhang Y, et al. "Change detection with multi-source defective remote sensing images based on evidential fusion". *ISPRS Annals of the Photogrammetry, Remote Sensing and Spatial Information Sciences*. 3(7), pp. 125-132, 2016.

[4] Neha J, Matthias B, Andrea E, et al. "A review of the application of optical and radar remote sensing data fusion to land use mapping and monitoring". *Remote Sensing*, 8(1), pp. 70-92, 2016.

[5] Chen X, Li J, Zhang Y, et al. "Evidential Fusion Based Technique for Detecting Landslide Barrier Lakes From Cloud-Covered Remote Sensing Images". *IEEE J. Sel. Topics Appl. Earth Observ. in Remote Sens*. 10(5), pp. 1742-1757, 2017.

[6] Liu Z, Pan Q, Dezert J, et al. "Combination of classifiers with optimal weight based on evidential reasoning". *IEEE Trans. Fuzzy Sys*. 26(3), pp. 1217-1230, 2018.

Authorized licensed use limited to: University of Cape Town. Downloaded on May 17,2021 at 19:01:25 UTC from IEEE Xplore. Restrictions apply.